

WHEN IS A QUANTUM GAS A QUANTUM LIQUID?

J. M. PINO, R. J. WILD, S. B. PAPP, S. RONEN, D. S. JIN, AND E. A. CORNELL

*NIST/JILA, University of Colorado,
Boulder, CO, 80309, USA*

**E-mail: cornell@jila.colorado.edu*

We report on measurements of the excitation spectrum of a strongly interacting Bose-Einstein condensate (BEC). A magnetic-field Feshbach resonance is used to tune atom-atom interactions in the condensate and to reach a regime where quantum depletion and beyond mean-field corrections to the condensate chemical potential are significant. We use two-photon Bragg spectroscopy to probe the condensate excitation spectrum; our results demonstrate the onset of beyond mean-field effects in a gaseous BEC.

Keywords: Bragg Spectroscopy; Beyond mean-field; Feshbach resonance.

The concept of an interacting but dilute Bose gas was originally developed fifty years ago as a theoretically tractable surrogate for superfluid liquid helium. For some years after the eventual experimental realization of dilute-gas Bose-Einstein condensate (BEC), experiments were performed mainly in the extreme dilute limit, in which atom-atom correlations were of negligible significance. Such correlations again assumed a central role, however, in the 2002 experiments on a Mott state for bosons in an optical lattice¹ and on atom-molecule coherence near a Feshbach resonance². Atom-atom correlations are also central to the current hot-topic field of resonant fermionic condensates^{3,4}.

In this paper we describe an experimental study of elementary excitations in a system which harkens back to a previous century, in that, like liquid helium, it is a strongly interacting, bulk, bosonic superfluid. Unlike liquid helium, our gas of Bose-condensed ⁸⁵Rb has the modern virtue of Feshbach-tunable interactions well-described by a scattering length a that is much larger than the reach of the actual interatomic potential. Our tool for characterizing the sample is Bragg spectroscopy^{5,6}.

Our experiments are performed using a ^{85}Rb BEC near a Feshbach resonance at 155 G^{7,8}. A gas of ^{85}Rb atoms in the $|F = 2, m_F = -2\rangle$ state is first sympathetically cooled with ^{87}Rb in a magnetic trap and then evaporated directly to ultralow temperature in an optical dipole trap⁹. We create a single-species ^{85}Rb condensate¹⁰, with 40,000 atoms and a condensate fraction greater than 85%, in a weakly confining optical dipole trap at a magnetic field above the Feshbach resonance where the scattering length is $150 a_0$. Curvature of the magnetic field enhances confinement along the axial direction of the optical trap. Following evaporative cooling, the optical dipole trap is recompressed and the final trap has a measured radial (axial) trap frequency of $2\pi \times 134$ Hz ($2\pi \times 2.9$ Hz), yielding a condensate mean density of $2.1 \times 10^{13} \text{ cm}^{-3}$.

Bragg spectroscopy via stimulated two-photon transitions provides a direct probe of the condensate excitation spectrum. Two counter-propagating, near-resonant laser beams are aligned along the long axis of the condensate. The momentum imparted to a condensate excitation is given by $\hbar k = 2\hbar k_L$ where $k_L = \frac{2\pi}{780 \text{ nm}}$ is the wave vector of a beam. The excitation energy is scanned by adjusting the frequency difference of the two laser beams. The average of the two frequencies is red detuned from atomic resonance by 4.2 GHz. The intensity and pulse duration of the Bragg beams are chosen so that the fraction of the condensate excited is less than 10%.

Just before performing the Bragg spectroscopy, we transiently enhance the condensate density by means of large amplitude radial and axial breathing modes, which we excite by modulating the magnetic field and thus the Feshbach-modified scattering length. The rates of the ramps are limited so the \dot{a}/a never exceeds $0.06\hbar/(ma^2)$. The scattering length is derived from measurements of the magnetic field and a previous measurement of the ^{85}Rb Feshbach resonance¹¹. Synchronized with the inner turning point of the radial oscillation, we ramp the scattering length to the value for a given measurement and then pulse on the Bragg beams. During the pulse, the cloud's inward motion is checked and it begins to breathe outward. We model the resulting time-dependent condensate density using a variational solution to the Gross-Pitaevskii equation¹², which predicts that the density of the cloud does not change by more than 30% during the Bragg pulse. We can meet this goal only by using progressively shorter Bragg pulses for higher values of desired a . The time- and space-averaged density during the pulse is approximately $7.6 \times 10^{13} \text{ cm}^{-3}$, but this depends weakly on the final value of a .

After the Bragg pulse, we ramp a to $917 a_0$ in order to ensure that the momentum of the excitations is spread via collisions^{13,14} to the entire condensate sample. We then infer the total momentum, and thus excitation fraction, from the amplitude of the resulting axial slosh, measured via an absorption image taken of the cloud at a time near its axial turning point.

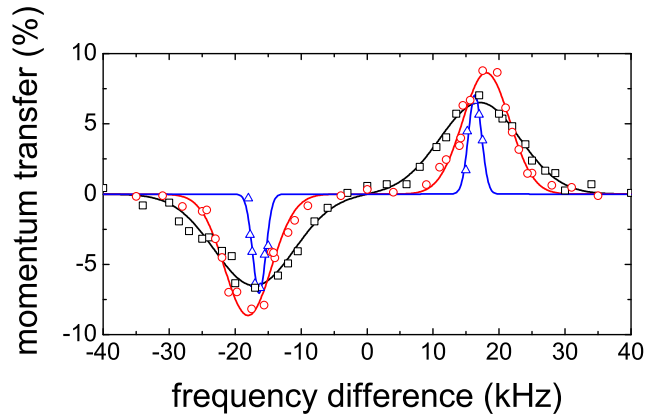


Fig. 1. Typical Bragg spectra at a scattering length of $100 a_0$ (blue triangles), $585 a_0$ (red circles), and $890 a_0$ (black squares). The excitation fraction is determined from the measured momentum transferred to the BEC and plotted as a function of the frequency difference between the two Bragg beams. Lines are fits of the data as described in the text. Mean-field theory predicts a continuous increase in the line shift with increasing a , however by $890 a_0$ our data display a *decreasing* shift with stronger interactions.

Figure 1 shows measured Bragg spectra for three values of a . We fit each Bragg spectrum to an antisymmetric function assuming a Gaussian peak and extract a center frequency and an RMS width. The Bragg line shift is the difference between the fitted center and the ideal gas result $\frac{1}{2\pi} \frac{\hbar k^2}{2m} = 15.423$ kHz. In Fig. 2a we plot our measured line shifts as a function of the scattering length a . For $a \lesssim 300a_0$ (where the predicted LHY correction is already a 10% effect), the measured line shift (\bullet in Fig. 2a) agrees with the simple mean-field result. However, as the scattering length is increased further, the resonance line shift deviates significantly from the mean-field prediction. The measured line shift reaches a maximum near $a = 500a_0$ and then *decreases* as the scattering length is increased further.

At large a we find that our measured line shift exhibits a systematic dependence on the temperature of the sample¹⁶. Non-condensed ^{85}Rb atoms also respond to the Bragg pulse, and this causes an observable effect in the

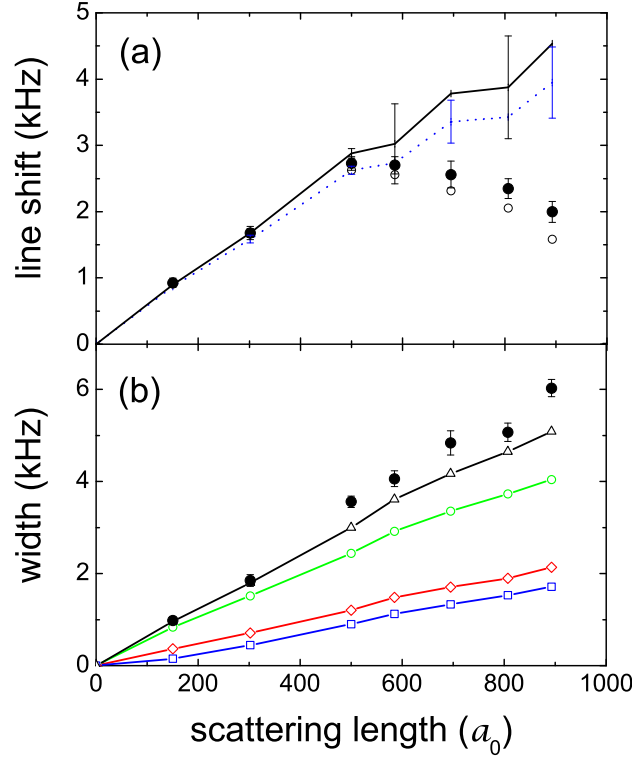


Fig. 2. (a) Bragg line shift and (b) width as a function of scattering length. In (a) the hollow circles are our observations. The solid circles are data corrected for a fitting systematic associated with the broad thermal atom background, and the error bars represent fit uncertainties. The solid black theory line corresponds to the simple mean-field shift $\propto na$, and the blue dotted line gives the full Bogoliubov¹⁵ theory, which includes phonon interactions. The theory lines are calculated for the trapped gas using a local density approximation for each of the corresponding data points. The mean BEC density ranges from $6.3 \times 10^{13} \text{ cm}^{-3}$ to $7.6 \times 10^{13} \text{ cm}^{-3}$. Error bars on the theory lines reflect uncertainty in these densities. Some of the error bars have been omitted for clarity. In (b) the solid black circles are the rms width of a gaussian fit to the Bragg spectra. Black triangles are from a fit to a convolution of various contributions to the width calculated under the conditions of our measurements. The remaining symbols characterize constituent contributions to the convolution including the Lorentzian FWHM width due to collisions (blue squares), and the RMS width of a Gaussian fitted to the contributions due to the inhomogeneous density (red diamonds) and the pulse duration (green circles). The largest contribution to the width comes from the pulse duration; because the jump to large a initiates rapid expansion of the BEC, ever shorter pulses are used to obtain the spectra at larger a .

measured line shift when the spectral width of the condensate response becomes comparable to that of the non-condensed atoms (for $a > 500a_0$). We vary the temperature of the gas to characterize this effect and we apply a small empirical correction to our data to represent the expected line shift at zero temperature (\bullet in Fig. 2a).

Figure 2b shows the measured width of the Bragg peak as a function of a . Several effects contribute to the total width of the Bragg resonance including the finite duration of the pulse, the inhomogeneous density of the trapped condensate⁵, collisions between the excitations and the condensate¹³, and Doppler broadening⁵. In our case, Doppler broadening is negligible since the axial size of the condensate is relatively large. To understand the total width we convolve the various calculated lineshapes of the remaining three effects. We fit a Gaussian to the convolution (to match the Gaussian fit to our data) and the RMS width from this fit is shown in Fig. 2b (black \triangle). Fig. 2b also shows the expected contributions to the width from each of the three effects. For the lineshape due to collisions we expect a Lorentzian with a full width at half maximum $\delta\nu = \frac{1}{2\pi} \frac{n\sigma k}{m}$, where σ is the elastic cross section for collisions between the excitations and low momentum atoms. In calculating σ we include the suppression in the phonon regime predicted by Beliaev^{17,13}. The measured Bragg width exceeds the predicted width in the strongly interacting regime. However, many of the theoretical difficulties in describing the line shift apply also to predicting the width that arises from inhomogeneous density and excitation lifetime.

A key future goal of our work is to experimentally explore different time-scales for the establishment of local many-body quasi-equilibrium, and for longer-term evolution. The extreme aspect ratio of our sample hastens the loss of density that occurs during the expansion caused by the ramp to high a . At present, we are required to use short duration Bragg pulses, which limits our spectral resolution, and we are prevented from tracking the time evolution of line shifts. An ongoing redesign to a more spherical geometry will help. In addition, the Bragg beams are being reconfigured to allow access to the low- k , pure-phonon regime for which $1/(k\xi) \gg 1$.

A more complete account of this work has appeared in S. B. Papp, J. M. Pino, R. J. Wild, S. Ronen, C. E. Wieman, D. S. Jin, and E. A. Cornell, Phys. Rev. Lett. **101**, 135301 (2008). We gratefully acknowledge useful conversations with J. Bohn, M. Holland, R. Ballagh, S. Stringari and the JILA ultracold atom collaboration. This work is supported by NSF and ONR.

References

1. M. Greiner *et al.*, Nature **415**, 39 (2002).
2. E. A. Donley *et al.*, Nature **417**, 529 (2002).
3. C. A. Regal, M. Greiner, and D. S. Jin, Phys. Rev. Lett. **92**, 040403 (2004).
4. M. W. Zwierlein *et al.*, Phys. Rev. Lett. **92**, 120403 (2004).
5. J. Stenger *et al.*, Phys. Rev. Lett. **82**, 4569 (1999).
6. D. M. Stamper-Kurn *et al.*, Phys. Rev. Lett. **83**, 2876 (1999).
7. S. L. Cornish *et al.*, Phys. Rev. Lett. **85**, 1795 (2000).
8. J. L. Roberts *et al.*, Phys. Rev. Lett. **85**, 728 (2000).
9. S. B. Papp and C. E. Wieman, Phys. Rev. Lett. **97**, 180404 (2006).
10. The number of trapped ^{87}Rb atoms remaining is $< 10\%$ of the ^{85}Rb number.
11. N. R. Claussen *et al.*, Phys. Rev. A **67**, 060701(R) (2003).
12. V. M. Pérez-García *et al.*, Phys. Rev. A **56**, 1424 (1997).
13. N. Katz *et al.*, Phys. Rev. Lett. **89**, 220401 (2002).
14. A. P. Chikkatur *et al.*, Phys. Rev. Lett. **85**, 483 (2000).
15. N. Bogoliubov, J. Phys. (Moscow) **11**, 23 (1947).
16. A. Brunello *et al.*, Phys. Rev. A **64**, 063614 (2001).
17. S. T. Beliaev, Sov. Phys. JETP, **34**, 299 (1958).
18. L. Pitaevskii and S. Stringari, Phys. Rev. Lett. **81**, 4541 (1998).
19. A. Altmeyer *et al.*, Phys. Rev. Lett. **98**, 040401 (2007).
20. J. Kinast, A. Turlapov, and J. E. Thomas, Phys. Rev. A **70**, 051401(R) (2004).
21. F. Dalfovo *et al.*, Rev. Mod. Phys. **71**, 463 (1999).
22. J. Steinhauer *et al.*, Phys. Rev. Lett. **88**, 120407 (2002).
23. R. Ozeri *et al.*, Rev. Mod. Phys. **77**, 187 (2005).
24. T. D. Lee and C. N. Yang, Phys. Rev. **105**, 1119 (1957).
25. T. D. Lee, K. Huang, and C. N. Yang, Phys. Rev. **106**, 1135 (1957).
26. P. Nozières and D. Pines, *The Theory of Quantum Liquids* Superfluid Bose Liquids Vol. II (Addison-Wesley, Redwood City, CA, 1990).
27. A. Griffin, *Excitations in a Bose-Condensed Liquid*, (Cambridge University Press, Cambridge, England, 1993).
28. J. Steinhauer *et al.*, Phys. Rev. A **72**, 023608 (2005).
29. E. Braaten, H. W. Hammer, and T. Mehen, Phys. Rev. Lett. **88**, 040401 (2002).
30. F. Mohling and A. Sirlin, Phys. Rev. **118**, 370 (1960).
31. S. Ronen, arXiv:0809.1448.